Inter-Radar Interference Mitigation by Multi-Channel RNN with Multi-head Self-Attention

Yudai SUZUKI
Graduate School of Science and Engineering
Ibaraki University
Hitachi, Japan
24nm630lf@vc.ibaraki.ac.jp

Xiaoyan WANG
Graduate School of Science and Engineering
Ibaraki University
Hitachi, Japan
xiaoyan.wang.shawn@vc.ibaraki.ac.jp

Masahiro UMEHIRA
Graduate School of Science and Engineering
Nanzan University
Nagoya, Japan
umehira@nanzan-u.ac.jp

***Abstract*— Automotive radar plays a crucial role in autonomous driving and road safety applications. However, the growing adoption of radar sensors leads to severe mutual interference among radars, significantly reducing the target detection rate. Numerous interference mitigation methods have been investigated in recent years. Recently, deep learning models have been applied to this challenging problem, showing promising performance compared to conventional methods. In this paper, we propose a multi-channel RNN with multi-head self-attention model for automotive radar interference mitigation. Specifically, we employ a bidirectional GRU (Gated Recurrent Units) model with two channels to process the real and imaginary parts of signals simultaneously, and utilize multi-head self-attention mechanisms to enhance the model's ability to focus on specific parts of the input signals. The performance is validated through extensive simulations, demonstrating superior results in terms of SNR (Signal-to-Noise Ratio), amplitude absolute error, phase absolute error compared to existing RNN models.**

Keywords*— *CS radar, inter-radar interference, wideband interference, RNN model, self-attention

I. INTRODUCTION

FMCW (frequency modulated continuous wave) and CS (chirp sequence) radars are among the most widely used in-vehicle sensors for autonomous driving and road safety applications. The mmWave (millimeter-wave) CS radar [1] is particularly popular as an automotive radar sensor due to its high resolution, compactness, cost-efficiency, and superior robustness to weather and ambient light conditions, compared with cameras and LiDAR (Light Detection and Ranging).

The CS radar performs dechirping operations on transmitted and received signals to detect the distance and velocity of nearby targets. With the growing adoption of mmWave radars, however, the probability of inter-radar interference [2] increases, leading to corrupted signals. Mutual interference among CS radars can be classified into two types: wideband interference [3], which occurs when the chirp rates of the victim radar and the interfering radar are different; and narrowband interference [4], which occurs when they are the same. Wideband interference degrades the target detection rate due to increased noise levels, while narrowband interference generates ghost targets. Since wideband interference is more frequent than narrowband interference, we focus on wideband interference in this work.

To mitigate wideband inter-radar interference, various approaches have been proposed, ranging from conventional algorithm-based methods to deep learning-based methods. The most basic yet widely used approach is zero-suppression, which identifies corrupted samples using a threshold and replaces the samples above this threshold with zero. Building on zero-suppression, several algorithm-based approaches [5] have been proposed, which dynamically set the threshold to handle different types of interference patterns. In recent years, deep learning-based approaches demonstrated high performance for various signal processing problems. Specifically, convolutional neural networks (CNNs) are utilized to mitigate inter-radar interference by operating on RD (range-Doppler) maps [6,7], while recurrent neural networks (RNNs) are used to reconstruct corrupted beat signals in the time domain [8,9]. Compared with conventional algorithm-based approaches, deep learning-based approaches can find a mapping between interfered and clean signals, and thus mitigate the interference in a threshold-free manner.

These existing deep learning-based methods either only utilize the real part of the signal, or treat the real and imaginary parts of the signal independently. However, overlooking the relationship between real and imaginary parts may result in a loss of phase information in the beat signal, which is important for measuring the velocity of the target.

In this work, we propose a multi-channel RNN with multi-head self-attention method to mitigate inter-radar interference. Specifically, we employ a bidirectional GRU (gated recurrent units) model with two channels to process real and imaginary parts of signals simultaneously, and utilize multi-head self-attention mechanisms to enhance the model's ability to focus on specific parts of the input signals. Extensive simulation results demonstrate the superiority of the proposed method in terms of SNR (signal-to-noise ratio), amplitude AE (absolute error), phase AE, compared to other existing RNN-based approaches [8,9].

The outline of this paper is as follows. In section II, principles of CS radar and wideband interference are

979-8-3503-5469-0/24/$31.00 ©2024 IEEE

described. Section III and IV present the proposed method and simulation results, respectively. Finally, Section V gives the conclusion remarks.

II. Principle of Wideband Interference

A. Priciple of Chirp Sequence Radar

The diagram of CS radar is shown in Fig. 1. The transmitted signal is a linear chirp sequence that follows a sawtooth pattern as shown in Fig. 2. The transmitted signal could be represented as Eqn. (1).

$$f_{\mathrm{Tx}}(t) = f_c + \frac{\Delta f}{\Delta T} t \tag{1}$$

where t is time, Δf is bandwidth, ΔT is chirp periods, and f_c is start frequency. The signal propagates and is reflected by targets, resulting in a received signal as described by Eqn. (2).

$$f_{\mathrm{Rx}}(t) = f_c + \frac{\Delta f}{\Delta T}(t - \tau_d) \tag{2}$$

$$\tau_d = \frac{2(R + Vt)}{c} \tag{3}$$

where τ_d is time delay, R and V are distance and velocity of the target respectively, and c is light speed. After dechirping and low-pass filtering, the beat frequency f_b represented by Eqn. (4) could be obtained.

$$f_b = \frac{2\Delta f R}{c\Delta T} + \frac{2V}{c} f_0 \tag{4}$$

Upon conducting a 2D-FFT on this beat signal, an RD map is generated, from which the distance and velocity of the target could be derived using Eqns. (5) and (6).

$$R = \frac{c\Delta T}{2\Delta f} \tag{5}$$

$$V = \frac{c}{2f_0} \tag{6}$$

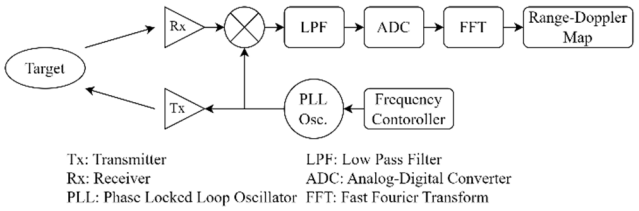

Fig. 1 Diagram of CS radar

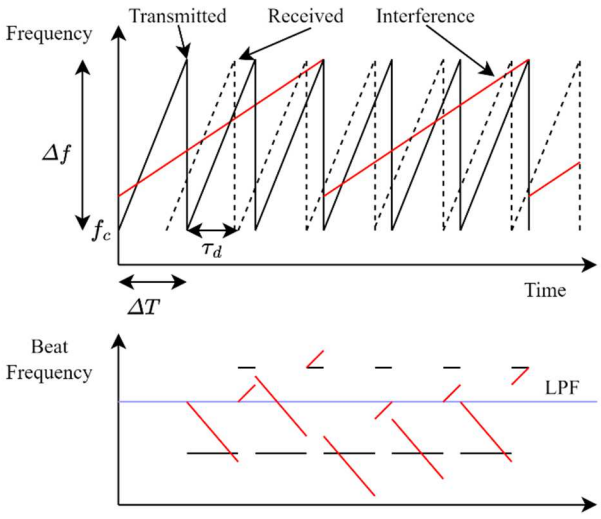

Fig. 2 Radar signal and beat frequency

B. Wideband Interference

When the radar signals from different vehicles are received, inter-radar interference occurs. The interfered beat signal is represented by Eqn. (7).

$$y(t) = s(t) + n(t) + i(t) \tag{7}$$

where $s(t)$ is desired signal, $n(t)$ is noise, and $i(t)$ is interference. As illustrated in Fig. 2, wideband interference occurs when the chirp rates of the victim radar signal and the interfering radar signal are different. As shown in Fig. 3, pulsed-like interference signals could be observed in the time domain because the received signal power from the interfering radar is generally much larger than that of reflected signal from the target. After FFT, this interference spreads across all frequencies in the frequency domain, resulting in increased noise level and thus a reduced target detection rate.

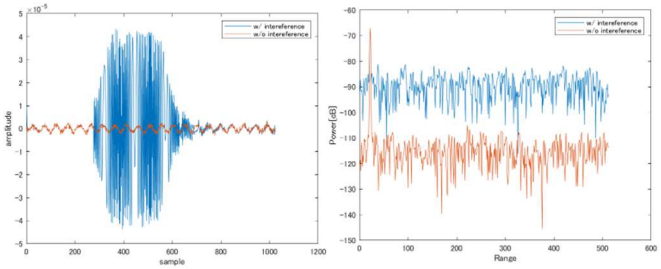

Fig. 3 Time waveform and range profile with and without interference

III. Proposed Interference Mitigation Method

In this section, we firstly present the preliminaries of bidirectional GRU and self-attention, which are used in our proposed method. Then, we introduce the proposed model followed by the explanations of loss function and training procedure.

A. Bidirectional GRU

RNNs are classes of the neural network that are suitable for learning sequential data. GRU is one of the improved RNN models that implemented two stochastic gates to capture long-term dependencies with more efficiency. For a GRU cell, the outputs at time step t are calculated by Eqns. (8) to (11).

$$r_t = \sigma(W_r x_t + U_r h_{t-1} + b_r) \tag{8}$$

$$z_t = \sigma(W_z x_t + U_z h_{t-1} + b_z) \tag{9}$$

$$\tilde{h_t} = \tanh\big(W_h x_t + U_h(r_t \odot h_{t-1})\big) + b_h \tag{10}$$

$$h_t = y_t = (1 - z_t) \odot h_{t-1} + z_t \odot \tilde{h_t} \tag{11}$$

where $W_r, U_r, W_z, U_z, W_h, U_r$ are learnable weights, b_r, b_z, b_h are learnable bias, x_t, y_t, h_t are respectively input, output, and hidden state at time step t, and the symbol $\odot$ is the Hadamard product, which computes the element-wise product of metrices. The reset gate r_t takes a value between 0 and 1 and is applied to the hidden states, controlling how much of the previous context is incorporated into the computation of the candidate hidden states $\tilde{h_t}$ at time step t. The update gate z_t also ranging from 0 to 1, weights the hidden state at time step $t-1$ and the candidate hidden state in the calculation of the new hidden state at time step t. The outputs of the recurrent layer are obtained by repeating these calculations across the entire sequence length.

Fig. 4 shows the structure of bidirectional GRU (biGRU). BiGRU is a variant of the GRU architecture that processes

input sequences in both forward and backward directions. By utilizing information from past and future contexts simultaneously, biGRU is capable of enhancing the model's ability to capture dependencies and patterns from both directions of beat signals in our interference mitigation task.

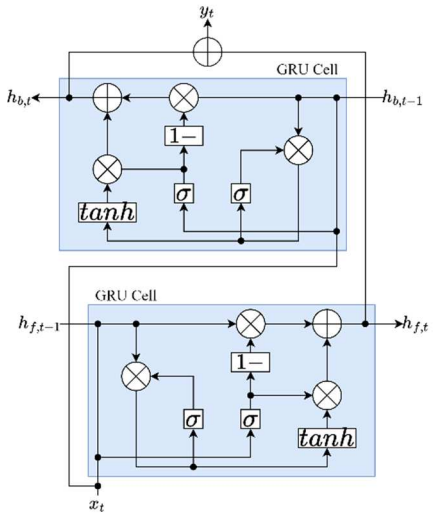

Fig. 4 Structure of biGRU

B. Self-Attention

We employ a self-attention mechanism [10] to capture the relationships among signal samples and between real and imaginary parts of the signals. Fig. 5 shows the self-attention architecture. First, the input vector $\boldsymbol{x}$ undergoes a linear transformation to obtain the query $\boldsymbol{Q}_i$, key $\boldsymbol{K}_i$, and value $\boldsymbol{V}_i$ for each of the h heads, as shown in Eqns. (12) to (14).

$$\boldsymbol{Q}_i = \boldsymbol{x}W_{Q_i} + \boldsymbol{b}_{Q_i} \tag{12}$$

$$\boldsymbol{K}_i = \boldsymbol{x}W_{K_i} + \boldsymbol{b}_{K_i} \tag{13}$$

$$\boldsymbol{V}_i = \boldsymbol{x}W_{V_i} + \boldsymbol{b}_{V_i} \tag{14}$$

where $W_{Q_i}, W_{K_i}, W_{V_i}$ are learnable weights, $\boldsymbol{b}_{Q_i}, \boldsymbol{b}_{K_i}, \boldsymbol{b}_{V_i}$ are learnable bias vectors, i is the head number. Afterward, these vectors are inputted into the Scaled Dot Product Attention Block. The attention weight matrix W_i of this block are computed by Eqn. (15).

$$W_i = softmax\left(\frac{\boldsymbol{Q}_i \boldsymbol{K}_i{}^T}{\sqrt{d_k}}\right) \tag{15}$$

where d_k is the dimension of query $\boldsymbol{Q}_i$ and key $\boldsymbol{K}_i$. The association between each sample is represented by calculating the product of the $\boldsymbol{Q}$ vector and the transposed $\boldsymbol{K}$ vector. Standardization is then performed by dividing all elements by the scale $\sqrt{d_k}$ for efficient learning. The attention weight W_i are obtained by applying the softmax activation function. The output $\boldsymbol{z}_i$ of the i-th head is computed by multiplying W_i with the value vector $\boldsymbol{V}_i$ as Eqn. (16).

$$\boldsymbol{z}_i = W_i \cdot \boldsymbol{V}_i \tag{16}$$

The outputs of all heads are concatenated and undergo a linearly transformation. This yields the final output of the self-attention mechanism. When the number of head h is one, we refer to this block as 'single-head self-attention'. When h is greater than one, we refer to it as 'multi-head self-attention'.

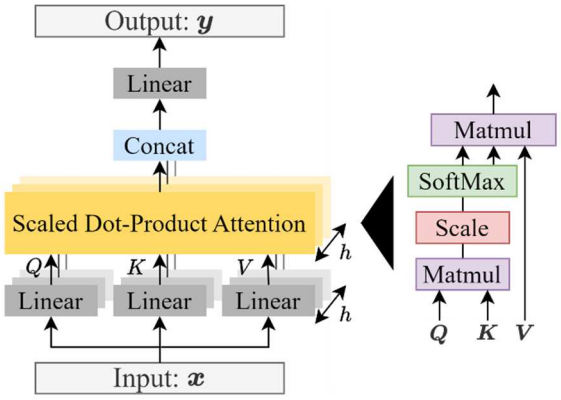

Fig. 5 Self-attention architecture

C. Proposed Model

Fig. 6 illustrates the architecture of the proposed multi-channel RNN with multi-head self-attention model, which consists of 3 RNN layers and two attention block layers. In the multi-channel RNN layer, the real and imaginary parts of the beat signals are separately input into biGRU cells. The outputs from these two biGRU cells are concatenated and fed into an attention block with 4 heads. The outputs of the attention block are split into two matrices, which serve as inputs to subsequent multi-channel RNN layers. Following the final RNN layer, average pooling is performed to obtain separate outputs for the real and imaginary components.

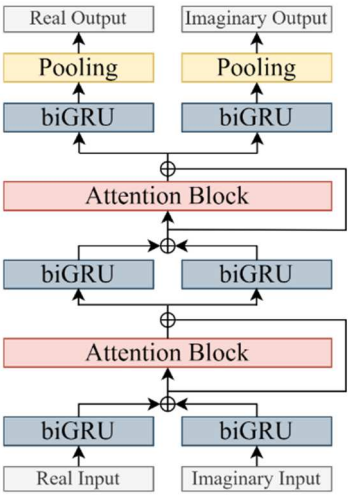

Fig. 6 Architectures of the proposed multi-channel RNN with multi-head self-attention model

D. Loss Function and Training Setup

Beat signals with interference are used as inputs, while corresponding interference-free signals serve as labels. We employ the MSE (mean squared error) as the loss function L, defined by Eqn. (17).

$$L = \frac{1}{N}\left(\sum_{n=1}^{N}(\hat{r}_t - r_t)^2 + \sum_{n=1}^{N}(\hat{\imath}_t - i_t)^2\right) \tag{17}$$

where r_t and i_t are real and imaginary labels, and $\hat{r}_t$ and $\hat{\imath}_t$ are real and imaginary outputs. The models are optimized by minimizing the loss L using the ADAM optimizer with a

learning rate of 0.001 and a batch size of 128 inputs. We train the models on 50 randomly generated scenarios, each consisting of 75 chirps. Table 1 displays the radar parameter setting ranges used in the simulation. All data is split into training and validation sets with a 9:1 ratio. The training process ends after 100 epochs.

Table. 1 Radar parameters

Parameters	Range
Center frequency	76~78GHz
Distance	1~130m
Velocity	1~50km/h
Chirp period	20~40μs
Sweep bandwidth	100~200MHz
Number of targets	1
Number of interferences	1~4

IV. Evaluation Results

In this section, we demonstrate the performance of the proposed method using synthetic CS radar signals. Firstly, we describe the evaluation metrics and comparison methods. For qualitative evaluation, we utilize time waveforms and RD maps. For quantitative evaluation, we measure the SNR, amplitude absolute error (AE) of targets, phase AE of targets, and processing time using Nvidia RTX A6000 GPU. 10 randomly generated scenarios are used for quantitative evaluations. We compare the proposed method with conventional zero-suppression, RNN with single-head self-attention [8,9], and RNN with multi-head self-attention. Notice that all the RNN models use biGRU cells.

Figs. 7 and 8 depict examples of time waveforms and RD maps before and after interference mitigation by different approaches. In the time waveform with interference, pulsed-like interference signals are evident. After zero suppression, it is clear that although the samples with large amplitudes are replaced by 0, a significant amount of interference still remains. From Figs. 7(d) to (f), we observe that all RNN with self-attention models efficiently mitigate interference and reconstruct corrupted signals. The proposed method notably outperforms existing methods, producing a waveform closest to the one without interference. Regarding the RD map with interference shown in Fig. 8(a), we observe that the potential target is completely obscured by noise. Zero suppression fails to mitigate interference in this scenario, due to the long interference duration. However, RNN with self-attention models significantly reduce noise levels and detect the target successfully. Specifically, the proposed method successfully mitigates noise across low-frequency ranges, which the other two RNN methods could not achieve.

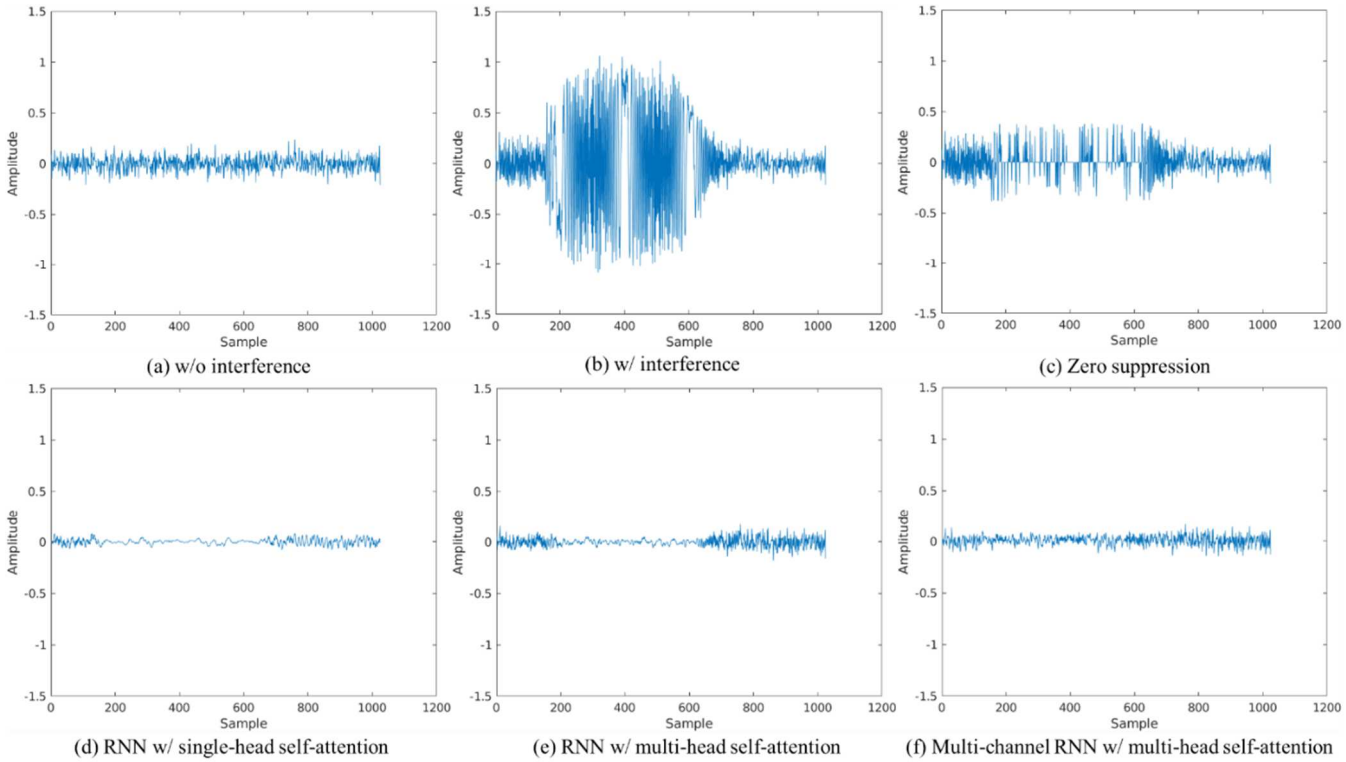

Fig. 7 Time waveform

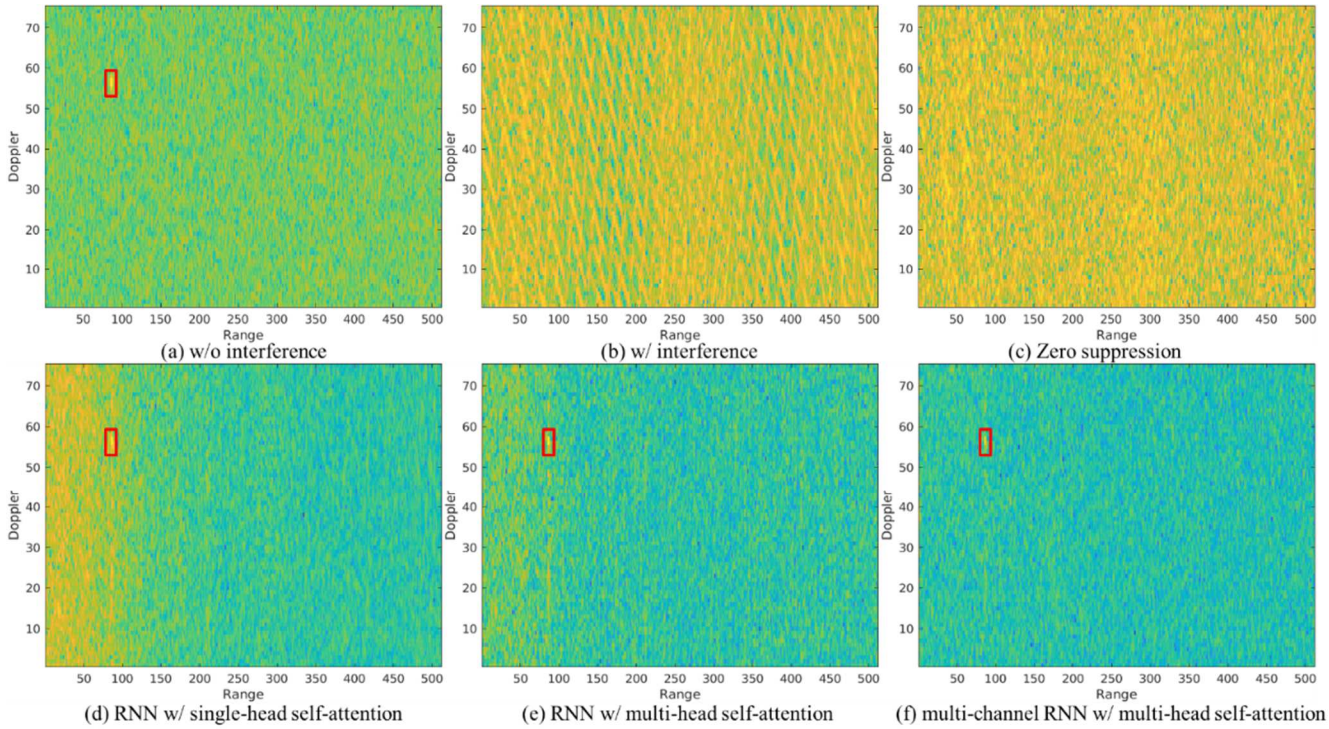

Fig. 8 Range Doppler map

Figs. 9, 10, and 11 indicate the cumulative distribution function (CDF) of SNR, amplitude AE and phase AE, respectively. In terms of SNR, the proposed method achieves performance closest to the SNR without interference, demonstrating the effectiveness of employing multi-head self-attention mechanisms and a multi-channel RNN model. Regarding amplitude AE, the proposed method also excels, with 80% of results showing amplitude AE below 10dB, highlighting its superior capability in reconstructing corrupted signal samples. In phase AE results, the proposed method consistently outperforms other approaches, enabling more accurate velocity measurement. Finally, as illustrated in Fig. 12, we confirm that the performance improvement of the proposed method comes with a longer processing time, which is as expected.

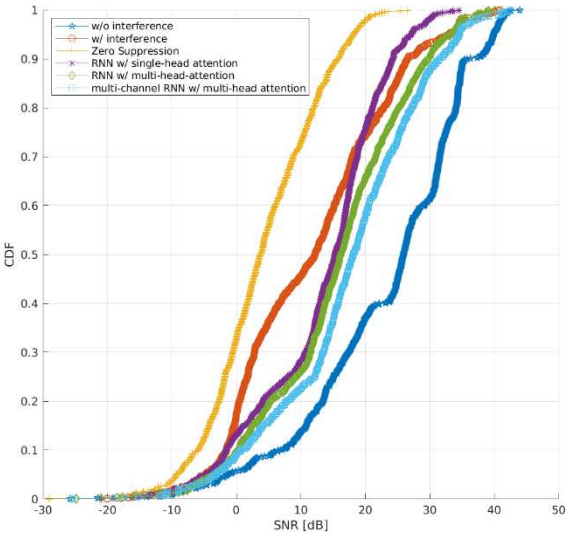

Fig. 9 CDF of SNR

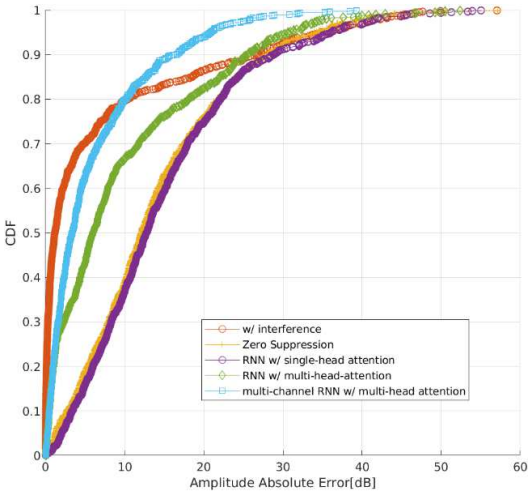

Fig. 10 CDF of amplitude absolute error

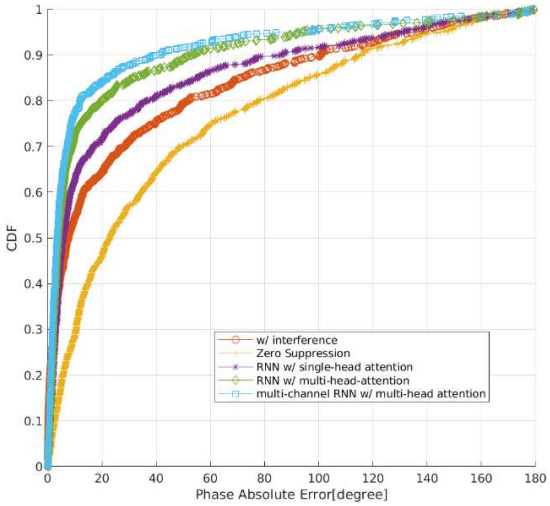

Fig. 11 CDF of phase absolute error

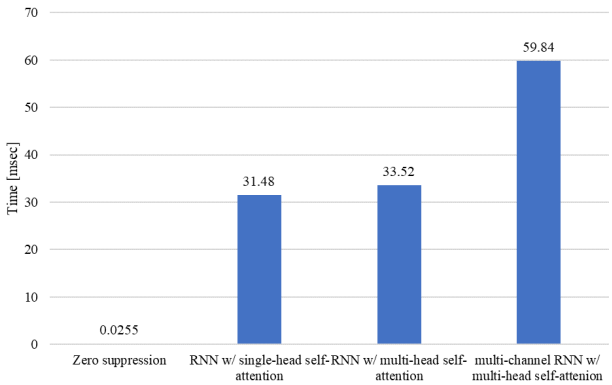

Fig. 12 Processing time

V. Conclusion

In this work, we propose a multi-channel RNN with multi-head self-attention model for the task of inter-radar interference mitigation. Extensive simulation results demonstrate that the proposed method outperforms existing RNN-based approaches in terms of SNR, amplitude AE, and phase AE. Moreover, we show that the proposed method is robust against low-frequency noise. In future work, we will further enhance the model by employing a custom loss function or multi-task learning and evaluate its performance using real-world experimental data.

Acknowledgment

This research and development work was supported by the MIC/SCOPE ## JP225003006.

References

[1] C. Waldschmidt, J. Hasch and W. Menzel, "Automotive Radar — From First Efforts to Future Systems," in IEEE Journal of Microwaves, vol. 1, no. 1, pp. 135-148, Jan. 2021.J. Clerk Maxwell, A Treatise on Electricity and Magnetism, 3rd ed., vol. 2. Oxford: Clarendon, 1892, pp.68–73.

[2] M. Umehira, Y. Watanabe, X. Wang, S. Takeda and H. Kuroda, "Inter radar interference in automotive FMCW radars and its mitigation challenges," 2020 IEEE International Symposium on Radio-Frequency Integration Technology (RFIT), 2020, pp. 220-222.

[3] Y. Makino, T. Nozawa, M. Umehira, X. Wang, S. Takeda and H. Kuroda, "Inter-radar Interference Analysis of FMCW radars with Different Chirp Rates", Journal of Engineering, vol. 2019, no 19, pp. 5634-5638, October 2019.

[4] D. Ammen, M. Umehira, X. Wang, S. Takeda and H. Kuroda, "A Ghost Target Suppression Technique using Interference Replica for Automotive FMCW Radars," 2020 IEEE Radar Conference (RadarConf20), 2020, pp. 1-5.

[5] M. Umehira, T. Okuda, X. Wang, S. Takeda, H. Kuroda, "An Adaptive Interference Detection and Suppression Scheme Using Iterative Processing for Automotive FMCW Radar," 2020 IEEE Radar Conference (RadarConf20), 2020, pp. 1-5.

[6] J. Rock, M. Toth, P. Meissner, and F. Pernkopf, “Deep interference mitigation and denoising of real-world FMCW radar signals,” in Proc. IEEE Int. Radar Conf. (RADAR), Apr. 2020, pp. 624–629.

[7] M. Hirschmugl, J. Rock, P. Meissner, F. Pernkopf, "Fast and resource-efficient CNNs for Radar Interference Mitigation on Embedded Hardware", 2022 19th European Radar Conference (EuRAD), pp.1-4, 2022.

[8] J. Mun, S. Ha, and J. Lee, “Automotive radar signal interference mitigation using RNN with self attention,” in Proc. IEEE Int. Conf. Acoust., Speech Signal Process. (ICASSP), May 2020, pp. 3802–3806.

[9] R. Koizumi, X. Wang, M. Umehira, R. Sun and S. Takeda, “Experimental Evaluations on Learning-based Inter-radar Wideband Interference Mitigation Method”, IEICE Transactions on Fundamentals of Electronics, Communications and Computer Sciences, Vol.E107-A,No.8,pp.-,Aug. 2024.

[10] A. Vaswani, N. Shazeer, N. Parmar, J. Uszkoreit, L. Jones, A. N. Gomez, Ł. Kaiser, and I. Polosukhin. 2017. “Attention is all you need” In Proceedings of the 31st International Conference on Neural Information Processing Systems (NIPS'17). Curran Associates Inc., Red Hook, NY, USA, 6000–6010.